Published in final edited form as:
Ultrasound Med Biol. 2009 March ; 35(3): 494–506. doi:10.1016/j.ultrasmedbio.2008.09.003.

Spatiotemporal Effects of Sonoporation Measured by Real-Time Calcium Imaging

R. E. Kumon[1,2], **M. Aehle**[2], **D. Sabens**[2], **P. Parikh**[2], **Y. W. Han**[3], **D. Kourennyi**[2], and **C. X. Deng**[1,2,*]

1 *Department of Biomedical Engineering, University of Michigan, 2200 Bonisteel Blvd., Ann Arbor, Michigan 48109–2099, USA*

2 *Department of Biomedical Engineering, Case Western Reserve University, 10900 Euclid Ave., Cleveland, Ohio 44106–7207, USA*

3 *School of Dental Medicine, Case Western Reserve University, 10900 Euclid Ave., Cleveland, Ohio 44106–4905, USA*

Abstract

To investigate the effects of sonoporation, spatiotemporal evolution of ultrasound-induced changes in intracellular calcium ion concentration ($[Ca^{2+}]_i$) was determined using real time fura-2AM fluorescence imaging. Monolayers of Chinese hamster ovary (CHO) cells were exposed to 1-MHz ultrasound tone burst (0.2 s, 0.45 MPa) in the presence of Optison™ microbubbles. At extracellular $[Ca^{2+}]_o$ of 0.9 mM, ultrasound application generated both non-oscillating and oscillating (periods 12–30 s) transients (changes of $[Ca^{2+}]_i$ in time) with durations of 100–180 s. Immediate $[Ca^{2+}]_i$ transients after ultrasound application were induced by ultrasound-mediated microbubble–cell interactions. In some cases, the immediately-affected cells did not return to pre-ultrasound equilibrium $[Ca^{2+}]_i$ levels, thereby indicating irreversible membrane damage. Spatial evolution of $[Ca^{2+}]_i$ in different cells formed a calcium wave and was observed to propagate outward from the immediately-affected cells at 7–20 μm/s over a distance greater than 200 μm, causing delayed transients in cells to occur sometimes 60 s or more after ultrasound application. In calcium-free solution, ultrasound-affected cells did not recover, consistent with the requirement of extracellular Ca^{2+} for cell membrane recovery subsequent to sonoporation. In summary, ultrasound application in the presence of Optison™ microbubbles can generate transient $[Ca^{2+}]_i$ changes and oscillations at a focal site and in surrounding cells via calcium waves that last longer than the ultrasound duration and spread beyond the focal site. These results demonstrate the complexity of downstream effects of sonoporation beyond the initial pore formation and subsequent diffusion-related transport through the cellular membrane.

Keywords

Sonoporation; Ultrasound; Calcium imaging; Calcium oscillations; Calcium waves; Microbubbles; Optison

*Corresponding author: Cheri X. Deng, Department of Biomedical Engineering, University of Michigan, 2200 Bonisteel Blvd, Ann Arbor, MI 48109–2099, USA. Tel: +1 734-936-2855; Fax: +1734-936-1905. E-mail address: E-mail: cxdeng@umich.edu (C. X. Deng).

INTRODUCTION

Sonoporation has been shown by many researchers to be a promising non-viral means for delivery of drugs, proteins, genes, and other agents into cells that would otherwise be impermeable (Ferrara et al., 2007; Miller et al., 2002; Paliwal and Mitragotri, 2006). In this process, it is likely that ultrasound produces transient, non-specific pores in the cell membrane, thereby permitting or enhancing the uptake of exogenous agents into the cytoplasm. Because non-ionizing ultrasound exposure can be non-invasively controlled in application location and duration, sonoporation may provide an advantageous, safe delivery strategy for targeted *in vivo* applications. However, despite the increasing interests and recent progress in the field (Bekeredjian et al., 2007; Feril et al., 2006; Hallow et al., 2007; Mehier-Humbert et al., 2007; Newman and Bettinger, 2007; Taylor et al., 2007; Tran et al., 2007; van Wamel et al., 2006a; Wu and Nyborg, 2007), a detailed understanding of the spatial and temporal processes and mechanisms involved in sonoporation remains to be fully determined (Campbell and Prausnitz, 2007). Furthermore, the molecular processes and mechanisms leading to subsequent cellular and organ effects have not been fully understood. By obtaining such an understanding, optimal sonoporation parameters may then be rationally determined and unwanted side effects mitigated, thus accelerating the successful translation of the technology to robust and safe clinical use.

Generally, studies of the efficiency of ultrasound-mediated drug and gene delivery and associated side effects, such as the loss of cell viability and enhanced apoptosis, have only been performed through post-ultrasound assays, which cannot characterize the detailed mechanisms of delivery and recovery. The challenge of studying sonoporation arises in part from the rapid time and microscopic length scales of the non-specific pore formation, which is often induced in practice via the use of excitation and collapse of oscillating microbubbles. As first steps in investigating the dynamical process of sonoporation, previous studies in our laboratory have used voltage clamp techniques to measure in real time the effects of ultrasound parameters such as acoustic pressure and duty cycle, as well as the extracellular calcium ion concentration ($[Ca^{2+}]_o$) on a single-cell model system, namely *Xenopus laevis* oocytes (frog eggs) (Deng et al., 2004; Zhou et al., 2008a; Zhou et al., 2008b). In particular, these studies have identified that Ca^{2+} is critically important for post-sonoporation pore resealing, which in turn determines delivery efficiency and cell survival. Our results are consistent with studies of cell repair of membrane wounding (McNeil and Steinhardt, 2003; Steinhardt, 2005; Togo et al., 1999; Togo et al., 2000) which revealed that the cell membrane repair is a highly regulated cellular process closely associated with extracellular Ca^{2+}.

These results suggested the importance of investigating the Ca^{2+} dynamics in response to sonoporation. As the result of formation of large and nonspecific pores (nm or μm) on the membrane induced by ultrasound exposure, transport of Ca^{2+} is likely to occur due to its concentration gradient across the cell membrane and may participate in or trigger significant and relevant cellular processes. Intracellular calcium transients and intercellular calcium waves are known to play a role in a variety of cell activities, including (but not limited to) oocyte fertilization, cell migration, gene expression, wound response, phagocytosis, and release of cytokines from epithelial cells (Berridge et al., 2003; Petty, 2006; Sanderson et al., 1994). For example, calcium waves have been found in migrating tumor cells, and an anti-metastatic drug has been shown to affect the calcium-wave properties of an invasive cancer cell line (Huang et al., 2004). Hence the specific study of Ca^{2+} effects has the potential to reveal the molecular mechanisms and cellular-level effects of sonoporation. The study can also provide important information about the spatial extent and temporal rate of cell poration and other ultrasound-induced effects. Such level of understanding may serve to guide optimization of this therapeutic modality by increasing delivery efficiency and post-sonoporation rate of cell survival.

By loading the cells with the Ca^{2+}-sensitive indicator dye fura-2 AM, which shifts its absorption spectrum upon binding to Ca^{2+} (Grynkiewicz et al., 1985), ratiometric fluorescence imaging of the intracellular calcium ion concentration $[Ca^{2+}]_i$ has been used to investigate calcium changes in cells. We have previously demonstrated the feasibility of employing this imaging technique to observe the effects of sonoporation in individual cells (Kumon et al., 2007b; Sabens et al., 2006) and have shown for the first time that ultrasound could induce Ca^{2+} transients and waves in cells in the presence of microbubbles (Kumon et al., 2007a). The current study focuses on the use of the real-time fluorescence imaging technique to obtain spatiotemporal information about Ca^{2+} during ultrasound-mediated sonoporation facilitated by microbubbles in the presence or absence of extracellular Ca^{2+}.

MATERIALS AND METHODS

Cell culture

Chinese Hamster Ovary (CHO) cells are epithelial-like cells commonly used as a mammalian cell model (Gamper et al., 2005). The CHO cells used for this study were cultured from the cells obtained from the American Type Culture Collection (ATCC, Manassas, VA). Cells were grown in 5 mL cell culture flasks following the vendor-provided standard protocol (ATCC, Manassas, VA), detached from the flask walls using a trypsin solution (1.5 mL of 0.05% trypsin, 0.53 mM EDTA), and then washed in Hank's balanced salt solution. The cell concentration was then adjusted to approximately 10^6 cells/mL, and the cells were immersed in Ham's F12K growth medium containing glutamine (ATCC recommended medium for the CHO cells is Kaighn's Modification of Ham's F-12 Medium which is modified to contain 2 mM L-glutamine and 1500 mg/L sodium bicarbonate. ATCC catalog number 30-2004), 10% inactivated fetal bovine serum, and gentamicin, prior to transfer to 35 mm cell culture dishes (BD Falcon351008, BD Biosciences, San Jose, CA). The dishes were stored in the incubator at 37°C and 5% CO_2 until approximately 70% confluency was achieved in 2 to 3 days.

Cell loading with Ca^{2+} indicator fura-2 AM

To image $[Ca^{2+}]_i$ levels, the cells were first loaded with the Ca^{2+} indicator fura-2 AM (Invitrogen F1221, Carlsbad, CA) prior to the ultrasound experiment. Fura-2 AM is a fluorophore that rapidly binds to Ca^{2+} in a 1:1 ratio and shifts its peak absorbance to lower wavelengths upon binding. The fura-2 AM solution was created by adding 10 μL of DMSO to 50μg of fura-2 AM. DMSO is initially used to reduce the premature spontaneous ester hydrolysis that can occur in moist environments. Next, 2 mL of a phosphate buffered saline (PBS) solution and 2 μL of 10% w/v Pluronic F-127 in water (Invitrogen P6686, Carlsbad, CA) was added to 2 μL of the fura-2 AM solution to yield a loading solution of 5 μM fura-2 AM. Pluronic F-127 is a detergent used to disperse the dye into the solution and thereby facilitate the loading of fura-2 AM into the cells. To load the cells, the growth medium was aspirated from the culture dish containing the cells, and then 0.66 mL of the loading solution was added to the cells. The cells were allowed to incubate in the loading solution at room temperature and in complete darkness for 60–90 min to maximize the fura-2 AM de-esterification necessary for Ca^{2+} binding. After loading, the cells were washed twice with the same PBS solution as used during the loading. The cells loaded with fura-2 AM were then placed in the test solution, which was a phosphate-buffered PBS solution with $[Ca^{2+}]_o = 0$ mM, or 0.9 mM, depending on the particular experiment. For the experiments with $[Ca^{2+}]_o = 0.9$ mM, the PBS solution contained 0.901 mM $CaCl_2$, 0.493 mM $MgCl_2$, 2.67 mM KCl, 137.93 mM NaCl, 1.47 mM KH_2PO_4, 8.06 mM Na_2HPO_4 (Dulbecco's PBS D8662, Sigma-Aldrich, St. Louis, MO, USA). A calcium free PBS (Dulbecco's PBS Modified 59321, Sigma-Aldrich, St. Louis, MO, USA) was used for the experiments with $[Ca^{2+}]_o = 0$ mM.

Ratiometric fluorescence imaging and data analysis

A microscopic ratiometric fluorescence imaging system was used to obtain the ratio of corresponding emitted fluorescence intensities at 510 nm from the fura-2AM using two different wavelength excitations (340 nm and 380 nm). The ratio of the emitted intensities from two excitation wavelengths, which is proportional to the $[Ca^{2+}]_i$, is measured because it is less sensitive to artifacts from uneven indicator distribution, photobleaching, and path length (Grynkiewicz et al., 1985) than use of a single wavelength. To perform real-time imaging, the light from a xenon lamp (Sutter Instrument Co. Lambda DG-4, Novato, CA) is rapidly directed through narrowband filters centered at 340 nm (for bound fura-2) and 380 nm (for unbound fura-2) which are alternated in the light pathway (Fig. 1). This excitation light is passed into an inverted microscope (Nikon Eclipse TE300, Melville, NY) with a Plan Fluor 20X ELWD (Nikon #45374) objective lens, and the subsequently emitted light from the cells due to the fura-2 fluorescence was then passed through an appropriate dichroic filter and an emission filter centered at 510 nm. The resulting series of photomicrographs were acquired with a 1392 × 1024 resolution cooled CCD camera (Photometrics Cool Snap HQ, Tucson, AZ) at 3 × 3 binning every 0.6 to 2 s for the duration of the experiment controlled by MetaFluor™ software (Molecular Devices, Downingtown, PA). Binning was employed to reduce the effects of noise and increase the rate of image acquisition.

The image analysis routines of MetaFluor™ (Molecular Devices, Downingtown, PA) were used for post-experiment image and data analysis. The emitted fluorescence intensities (at 510 nm) for both excitation wavelengths 340 nm and 380 nm (F_{340}^{raw},F_{340}^{raw}) in each cell was determined from manually segmented regions of the cell in the images. Cells that moved after the start of imaging or ultrasound treatment were excluded from the study. The background-corrected emitted fluorescence intensities at 510 nm from each excitation wavelength (F_{340}^{bg},F_{380}^{bg}) were obtained by subtracting the background fluorescence intensity (a region not containing fluorescence or cells). The ratio was then computed as $R=F_{340}/F_{380}=(F_{340}^{raw}-F_{340}^{bg})/(F_{380}^{raw}-F_{380}^{bg})$. The ratio for a segmented region was taken to be the average of the ratios computed at each pixel location within the area. The change in the ratio value in general indicates changes in $[Ca^{2+}]_i$. For example, an increase in $[Ca^{2+}]_i$ will result in an increase in the ratio value ($R=F_{340}/F_{380}$) because more fura-2 will be bound to Ca^{2+} resulting in an increase of the emitted fluorescence intensity at 510 nm from 340 nm excitation (F_{340}), while less fura-2 will be unbound to Ca^{2+} resulting in a decrease of the emitted intensity at 510 nm from the 380 nm excitation (F_{380}).

Ultrasound system and application

The ultrasound system used for the experiment consisted of a non-focused circular transducer specially-designed and made for our study (1 MHz center frequency, 0.25 inch active element diameter, Advanced Devices, Wakefield, MA). The transducer was driven by a function/waveform generator (Agilent Technologies 33250A, Palo Alto, CA) and a 75 W power amplifier (Amplifier Research 75A250, Souderton, PA). Due to the physical constrains of the experimental setup and the ultrasound duration (0.2 s), standing waves were expected to be present in the dish. The actual acoustic pressure close to the bottom of the dish under the experimental condition was measured using a calibrated L-shaped needle hydrophone (NP10-1A90, Ridgefield, CT) or a 40 μm calibrated needle hydrophone (Precision Acoustics HPM04/1, UK) through a small hole drilled on the dish bottom.

After the cells loaded with fura-2 AM were washed, 7 to 10 mL of PBS solution was added in the dish. The transducer was positioned such that the active surface of the ultrasound transducer submerged in solution was about 4 mm from the cells at the bottom of the dish and the insonified area included cells in the microscope's field of view. A 10% v/v solution of Optison™

(Amersham Health Inc., Princeton, NJ) was then added to the dish and mixed in solution. A 0.2 s tone burst ultrasound (peak negative pressure amplitude ~0.3 to 0.45 MPa) was applied to the cells to facilitate sonoporation. Fluorescence imaging was performed continuously to include measurements before, during, and at least 10 min after ultrasound application.

RESULTS

The effects of sonoporation or ultrasound application were represented as changes in the $[Ca^{2+}]_i$ as expressed by the images of the ratio value

$R=F_{340}/F_{380}=(F_{340}^{raw}-F_{340}^{bg})/(F_{380}^{raw}-F_{380}^{bg})$, where F_{340}^{raw} and F_{340}^{raw} are the emitted fluorescence intensities at 510 nm from 340 nm and 380 nm excitation respectively, as described in previous section. The fluorescence image pairs resulting from 340 nm and 380 nm excitation were consecutively acquired for control groups and test groups to obtain measurements before, during, and after ultrasound application. For the cells in control groups and the cells before ultrasound application, the ratio values remained essentially unchanged as a function of time. Variations in the equilibrium ratio values were observed to occur between cells, due in part to uneven dye loading and intrinsic differences between individual cells.

Ca^{2+} transients and waves from sonoporation in the presence of physiological $[Ca^{2+}]_o$

Ca^{2+} transients in individual cells—Ca^{2+} imaging of cells exposed to ultrasound application was performed in a solution of $[Ca^{2+}]_o$ = 0.9 mM, with and without the introduction of Optison™ microbubbles. Ca^{2+} transients, or changes in $[Ca^{2+}]_i$, of various characteristics were readily generated and observed in cells exposed to ultrasound field with microbubbles added in the solution. In comparison, for control groups, no significant changes in $[Ca^{2+}]_i$ of comparable magnitude were observed in the cells without ultrasound application or in the cells exposed to ultrasound (0.2 s, 0.45 MPa) in the absence of microbubbles in the solution, thereby suggesting that the interaction between the ultrasound, microbubbles, and cells was responsible for the detected $[Ca^{2+}]_i$ transients.

Several types of responses resulting from ultrasound application were observed, as shown by the example in Fig. 2. Figure 2A shows a fluorescence image (510 nm) resulting from 380 nm excitation prior to the application of ultrasound. (The brighter spots within the cells may be the result of uneven distribution of the fura-2 AM within intracellular organelles.) Responses include apparent overall increase in the fluorescence ratio after ultrasound application followed by a return to equilibrium with or without superimposed oscillations (Fig. 2B), as well as large and distinct oscillations with a less pronounced overall increase and decay in the baseline (Fig. 2C). Other adjacent cells exhibited one or both of these kinds of responses.

Generally, starting at the time of ultrasound application (e.g. t = 199 s in this case), the ratio values rapidly increased over 3 to 8 s (5.6 ± 2.3 s, n = 26), followed by a recovery to the pre-ultrasound values over 100 to 170 s (120 ± 20 s). Peak ratio values were in the range 1.5 to 2.7 (2.3 ± 0.3) or 375% to 900% (550% ± 120%) increase over the initial (equilibrium) ratio value. These values were typical for other cells in the field of view. The oscillation periods were in the range 12 to 30 s, typically lasting 3 to 6 cycles before oscillation stopped.

A notable finding is that the initial increase in $[Ca^{2+}]_i$ exhibited various delays in different cells. For example, cell 1 (circled in red) in Fig. 2A responded almost immediately at the time of the ultrasound pulse, and the other adjacent cells were delayed by 2 to 10 s, as can be seen more clearly in Fig. 2D. (Recall that the ultrasound lasts for 0.2 s.) The response was not necessarily a function of distance from Cell 1 as the more distal Cell 2 responded before Cells 4 and 5.

Calcium waves—The delays exhibited in the $[Ca^{2+}]_i$ transients appeared to originate from the propagation of a "calcium wave," as shown by a series of time-lapse ratio images (Fig. 3). These images were formed by coloring the hue at each pixel according to the ratio value and then modulating the intensity of the hue by the intensity of the corresponding image resulting from the 340 nm excitation. This conventional "intensity-modulated display" helps to suppress noise in the areas without fluorescence while retaining the information in the cell regions. (For reference, Fig. 3A shows the cells prior to the application of the ultrasound pulse, the white box corresponds to the approximately same set of cells as in Fig. 2A, and the white arrow points to Cell 1 in that figure.) An intracellular calcium wave was seen to propagate across the cell during the first 2 s after the ultrasound was applied (Fig. 3B–D) with an estimated wave speed of 12–14 μm/s. The intercellular propagation of the wave, primarily in cells left of Cell 1, was consistent with the initiation of the intracellular wave first observed on that side of Cell 1 (Fig. 3E–G; starting with Fig. 3G the field of view expands to the area below Cell 1.) The later expansion of the wave was seen to reach cells on both sides of Cell 1 (including Cells 4 and 5 in Fig. 2C); subsequently other waves propagate into the field of view from the lower left and lower right corners of the image (Fig. 3H–I). The origin of these waves could be one or more bubble-initiated sonoporation events outside the field of view.

The wavefronts of the spatial evolution of $[Ca^{2+}]_i$ changes do not affect all cells equally (i.e. some cells do not respond immediately when the front passes) and the wave appears to propagate at least in part from cell to cell (i.e, not by a broad, uniform wave front), as can be seen by the apparent spatial pathways of higher ratio cells, particularly in Fig. 3I (arrows). The wave speed of the intercellular waves was estimated to be in the range 7–20 μm/s, depending on the region and direction of propagation. Nearly all cells experienced some change in $[Ca^{2+}]_i$ 60 s after the ultrasound application (Fig. 3J), and eventually all recovered fully at 180 s (Fig. 3K and Fig. 3L), as compared to pre-ultrasound Fig. 3A, including Cell 1.

The contrast between the cases with readily generated and observed $[Ca^{2+}]_i$ transients in cells exposed to ultrasound in the presence of Optison™ microbubbles and the control cases (where no ultrasound was applied and where no microbubbles were added with or without ultrasound application) with no $[Ca^{2+}]_i$ significant changes, suggests a causal relationship of microbubbles in causing the $[Ca^{2+}]_i$ changes with ultrasound application. Some sequences of images showing microbubbles disappearance immediately after ultrasound exposure suggest more directly the role of microbubbles in the $[Ca^{2+}]_i$ changes at the time of ultrasound exposure. Figure 4A–C shows frames from a sequence of 380 nm excitation images immediately prior to the application of ultrasound. The white arrows point to a microbubble, drifting slowly (2–3 μm/s) above the cells for 14 s before ultrasound is applied. As it was out of the optical focus (which was placed on the cells below), the bubble appeared larger than the mean diameter of Optison™ bubbles of 2–3 μm. In the final frame before ultrasound application, the bubble is immediately adjacent to Cell 1 in Fig. 2, and the bubble is no longer seen in the image after the ultrasound application (Fig. 4D; at same time as Fig. 3A) while Ca^{2+} transients occurred in the immediate vicinity, suggesting that the bubble may have been destroyed and caused the Ca^{2+} response (Fig 4E–F; also Fig. 3). The bubbles' spherical shape and movement through the fluid above the stationary cells are better appreciated in the video sequence than the still images.

Failure of $[Ca^{2+}]_i$ recovery—As illustrated in Fig. 5, some cells failed to recover after ultrasound application. The time-evolution ratio traces (Fig. 5B) corresponding to the marked cells in the 380 nm excitation image (Fig. 5A) show that Cell 1 responds immediately at the time of the ultrasound pulse (t = 1035 s), and does not recover (Fig. 5B) while adjacent Cells 2 and 3 respond after delays of 4–5 s, long after the 0.2 s ultrasound pulse has ended, and show similar but smaller amplitude increase and recovery. Cell 2 recovers after 75 s and has two oscillations with period of 25 to 30 s, while Cell 3 recovers after about 20 s without oscillations. While most cells had similar recovery times, there were some cells that showed a significantly

slower recovery over 150 to 170 s (Fig. 5C), both without (Cell 4) and with oscillations (Cell 5; 25–40 s period). In still other cells, there was little to no response at all (data not shown).

To better understand the non-recovery response of Cell 1 in Fig. 5A, background-corrected fluorescence intensity traces (at 510 nm) with 340 nm and 380 nm excitation for Cells 1–3 in Fig. 5 were examined in more detail (Figs. 5D–E). While the ratio appears to reach a saturating ratio value (corresponding to a high $[Ca^{2+}]_i$), both intensities (at 340 nm and 380 nm excitation respectively) decrease after the ultrasound application for Cell 1, which is not the expected behavior for an increase of $[Ca^{2+}]_i$ alone (wherein the emitted intensity from 340 nm excitation should increase due to more fura-2 bound to Ca^{2+}, while the emitted intensity at 510 nm from the 380 nm excitation should decrease due to less fura-2 unbound to Ca^{2+}). In contrast, Cells 2 and 3 show an initial decrease of intensity from the 380 nm excitation and corresponding increase of intensity from the 340 nm excitation followed by the simultaneous reversal of these trends during the recovery to equilibrium. The dashed lines in Figs. 5D–E give the intensities from a small square region adjacent to Cell 1 where no cell is present and show that the intensities decrease to the level of the background or slightly above. Observation after the experiment showed that no morphological changes or detachment occurred for Cell 1 resulting from the ultrasound pulse. Photo-bleaching does not play a significant role in the decrease because other nearby cells, which were unaffected by the ultrasound, showed only a much lesser and slower drop in the fluorescence intensities from both 340 nm and 380 nm excitation (bleaching rate < 2%/min) as compared to the sudden change after the application of ultrasound. This result suggests that the decrease of fluorescence in cell (Cell 1) after the initial increase is due to fura-2 AM leakage or quenching, possibly a result of significant membrane damage from ultrasound-driven microbubble activities.

Further examination of the time-lapse ratio images for the data in Fig. 6 again reveals the propagation of a calcium wave originating from a single cell. (For reference, the white box in Fig. 6 corresponds to the approximately same set of cells as in Fig. 5A, while the white arrow points to Cell 1 in that figure.) The increased ratio of Cell 1 was visible in the first frame after the application of ultrasound (Fig. 6B), followed by the approximately elliptical expansion of the wave from the initial cell (Fig. 6C–G). The wave propagation was anisotropic, at least in part because some cells experience little or no change in $[Ca^{2+}]$, and, appear to partially block or slow down the propagation of the wave to subsequent cells. Intracellular wave propagation speeds were in the range 7–10 μm/s depending on propagation direction. The cells started to recover after the wave passes (Figs. 6G–H), and eventually the intracellular Ca^{2+} concentrations of nearly all cells returned to near their original levels (Fig. 6I), except for the cell that was immediately responsive (white arrow). The cell does not retain a red hue in the image because its intensity is suppressed by its low fluorescence from the 340 nm excitation in the image-modulated display.

$[Ca^{2+}]_i$ transients in the absence of extracellular Ca^{2+}

Ultrasound-mediated $[Ca^{2+}]_i$ transients were also observed in cells in calcium-free solution ($[Ca^{2+}]_o$ = 0 mM) with microbubbles. The cells were originally cultured under physiological $[Ca^{2+}]_o$, but they were less adherent to the dish surface and had lower confluency after being placed in the $[Ca^{2+}]_o$ = 0 mM solution, as seen in the 380 nm excitation fluorescence image prior to the application of ultrasound at t = 222 s (Fig. 7A). The ratio traces of Cells 1–3 in Fig. 7A initially dropped at the time of the ultrasound treatment (Fig. 7B), consistent with the transport of the Ca^{2+} out of the cell. The ratio subsequently increases to a saturating value with the time scale to saturation varying from 80 s (Cell 1) to 540 s (Cell 3). No oscillations or waves were observed in cells in the Ca^{2+}-free solution in our experiments with multiple sets of cells tested.

The background-corrected fluorescence (510 nm) intensity traces from 340 nm and 380 nm excitation (Fig. 7C–D) were also examined. The curves for Cells 2 and 3 show that the fluorescence intensity from 380 nm excitation initially increases and the fluorescence intensity from 340 nm excitation initially decreases, as would be expected for an initial drop in $[Ca^{2+}]_i$. However, both the intensities from 340 nm and 380 nm excitations continued to drop thereafter towards the background fluorescence level (represented by the dashed curves), suggesting that the subsequent increase in the ratio seen in Fig. 7B was not primarily due to an increase in $[Ca^{2+}]_i$, but due to dye leakage or quenching, possibly from a non-recovering damaged membrane. Photo-bleaching should not be the cause because other cells which were unaffected by the ultrasound pulse exhibited little drop in both fluorescence intensities from 340 nm and 380 nm excitation (bleaching rate < 1%/min). This behavior is thus reminiscent of the recovery failure observed in Cell 1 of Fig. 4.

DISCUSSION

This study shows the detailed spatiotemporal responses of mammalian cells to ultrasound application in the presence of microbubbles (Optison™). The ultrasound-induced cellular responses included a variety of $[Ca^{2+}]_i$ transients as well as intracellular and intercellular calcium waves. Possible mechanisms for these novel findings of sonoporation-related calcium-ion transients, oscillations, and waves are discussed next in more detail.

Plasma membrane poration and Ca^{2+} mechanotransduction

At physiological $[Ca^{2+}]_o$, ultrasound application caused immediate $[Ca^{2+}]_i$ transients in some cells, followed by delayed initiation of $[Ca^{2+}]_i$ transients in other surrounding cells. The delay time can be up to a minute or more, much beyond the duration of ultrasound application (0.2 s). The substantial increase in $[Ca^{2+}]_i$ in 0.9 mM $[Ca^{2+}]_o$ solution (Fig. 2, Cell 1) and decrease in $[Ca^{2+}]_i$ in 0 mM $[Ca^{2+}]_o$ solution (Fig. 7, Cells 2 and 3) immediately after ultrasound application strongly suggest that Ca^{2+} transport is occurring between the intracellular and extracellular spaces due to the ion concentration gradient through non-specific pores on the membrane.

Possible mechanisms involved in such microbubble-mediated pore formation in sonoporation include a combination of dynamic, complex processes such as shock waves from bubble collapse, fluid microjets from asymmetric bubble collapse near a physical boundary, rapid impact and penetration by ballistic shell-fragment resulted from bubble destruction, shear forces from oscillating microbubbles, collisions or coalescence of translating microbubbles with cells, and cavitation-induced chemical damage (Kudo et al., 2002; Ohl et al., 2006; Postema et al., 2004; Prentice et al., 2005; Sundaram et al., 2003; van Wamel et al., 2006b). While the fluorescence images in the current study do not have sufficient temporal resolution to see the time-resolved oscillations or collapse of individual microbubbles, images from the current and previous studies (Kumon et al., 2007a) suggest at least in some cases that the microbubbles were destroyed in the vicinity of cells that subsequently exhibited $[Ca^{2+}]_i$ transients. In these cases, microbubbles that were present prior to ultrasound application were either not present afterwards or dissolved into the surrounding medium subsequent to ultrasound application. Post ultrasound examination confirmed that > 98% of the Optison™ bubbles in the solution were destroyed under our experimental conditions. Similar to observations by ultra-high-speed photography for free microbubbles (Postema et al., 2005) and microbubbles adjacent to a cell monolayer (Prentice et al., 2005), microbubble destruction is likely to be the cause of the $[Ca^{2+}]_i$ transients observed immediately at the time of ultrasound application.

While other mechanisms such as active transport via endocytosis have been proposed for ultrasound-mediated uptake of extracellular agents facilitated by the presence of microbubbles,

increasing evidence points toward passive transport through non-specific nanoscale pores and/or larger physical disruption of the membrane because of the relatively large scale of observed pores (sometimes micron size), the long time scales often required for full recovery (tens of seconds to minutes), and the observed necessity of sufficient extracellular Ca^{2+} and energy to achieve full recovery (Schlicher et al., 2006; Zhou et al., 2008b).

Once non-specific pores on the cell membrane are created, Ca^{2+} transport across the membrane can occur by diffusion from or to the extracellular solution through these pores, as demonstrated by the occurrence of Ca^{2+} flux even when voltage-dependent Ca^{2+}-channels are blocked using verapamil in sonoporation in the types of cells with L-type Ca^{2+}-channels (Honda et al., 2004; Juffermans et al., 2006). These and our results show that the initial (direct) response is dominated by the value of the $[Ca^{2+}]_o$ relative to the $[Ca^{2+}]_i$. Similar to these results, the change of $[Ca^{2+}]_i$ (at least the very initial change) is due to outflux/influx through membrane, rather than from release from internal stores/buffers (e.g., endoplasmic reticulum, mitochondria, buffering proteins) or calcium channels.

The L-type calcium channels are a type of voltage-dependent calcium channel (VDCC). These voltage-gated Ca^{2+} ion channels are mostly found in excitable cells (*e.g.*, muscle, glial cells, neurons, etc.). At physiologic or resting membrane potential, VDCCs are normally closed. They are activated (*i.e.*, opened) at depolarized membrane potentials to allow Ca^{2+} entry into the cell. Results from a recent study by Tran et al. (Tran et al 2008) show that the influx of calcium in sonoporation does not depolarized membrane potential (breast cancer cells issued from MDA-MB-231 cell lines) to sufficient levels for activating these calcium channels. It is not expected that the L-type calcium channels present a major issue with the CHO cells used in this study.

The rise time for the transients observed in our study was in a similar range (3 to 10 s) for most of the cells observed. Insomuch as the mechanism at work is non-specific pore formation, the rise time places an upper bound on the length of time that the pore expanded before resealing. The actual duration over which a pore expanded to maximum size is most likely less, as some time is required for the initial influx of Ca^{2+} to diffuse or flow into the rest of the cell or for there to be a release of Ca^{2+} from internal stores and buffers.

Based on the translational motion of microbubbles in the fluid, the fluid velocity was estimated to be < 2 μm/s and was not correlated with the direction of calcium wave propagation. Thus the shear stresses from bulk flow of the fluid, either through incidental mixing from the translational movement of the microbubbles or from ultrasound-induced bulk fluid streaming probably do not play a significant role in the results of the current study.

Finally, Ca^{2+} transients can also occur due to mechanotransduction alone (i.e, without the creation of a non-specific pore), as shown in examples of direct mechanical contact (Enomoto et al., 1992; Sanderson et al., 1990), fluid flow (Davies, 1995; Geiger et al., 1992; Yellowley et al., 1997), and ultrasound in the absence of microbubbles (Kono et al., 2006; Mortimer and Dyson, 1988; Parvizi et al., 2002; Tsukamoto et al., 2005). While repeated trials have suggested that calcium response occurs in the presence of microbubbles, the current fluorescence imaging apparatus is limited such that it is difficult adequately capture of the rapid process of interactions between cells and micron-sized bubbles. It may be possible that ultrasound or ultrasound-mediated microbubble interaction could result in localized stresses without necessarily creating a pore for diffusive transport of Ca^{2+}, yet still trigger one of the mechanisms leading to Ca^{2+} transients, but additional experiments will be needed to determine the prevalence of this effect and specific molecular pathways involved.

Ca^{2+} oscillations and cell recovery

Our results show that ultrasound-induced $[Ca^{2+}]_i$ changes reach an extrema rapidly (3–5 s) followed by a slower process to return to an equilibrium level. In some cases, oscillations were observed to occur during the recovery, particularly in cells surrounding the initially sonoporated cells (cells immediately-affected by ultrasound-microbubble interaction).

The concurrent and pronounced decrease (significantly larger than changes due to photo-bleaching) of both the emitted fluorescence intensities from 340 nm and 380 nm excitations in some cells suggests dye loss and irreparable membrane damage. The highly localized and immediate damage to individual cells amidst a large number of still viable cells observed in our study suggests that direct interaction of a cell with only one or a few microbubbles is the cause for substantial and irreversible changes in these cells. Failure of cells to recover when $[Ca^{2+}]_o = 0$ mM in the current study suggests that Ca^{2+} is required during membrane resealing, consistent with results in *Xenopus laevis* oocytes (Deng et al., 2004; Zhou et al., 2008b), H9c2 rat cardiomyoblast cells (Juffermans et al., 2006), and human myelomonocytic lymphoma U937 cells (Honda et al., 2004). Research on mechanical cell membrane wounding (e.g. by micropipette) has shown that cells heal via an active, Ca^{2+}-dependent process that involves fusion of plasma membrane compartments with the plasma membrane at the wound site along with reorganization of the underlying cortical cytoskeleton (McNeil and Kirchhausen, 2005; McNeil and Steinhardt, 1997).

Calcium waves

While the detailed mechanisms of calcium waves is still a subject of extensive study, most evidence points toward (1) the transmission of an intracellular messenger (e.g., IP3 or Ca^{2+}) from one intracellular space to another through gap junctions (Boitano et al., 1992) or (2) the release of an extracellular messenger (e.g., ATP, ADP, and NO) which travels through the extracellular space from cell to cell (Sauer et al., 2000). It is possible that both are at work in the current study. In general that the variety of Ca^{2+} responses of individual cells to stimulation may be due to many factors, including inherent differences in the cells, e.g., so-called “calcium fingerprints” (Evans and Sanderson 1999; Godin et al. 2006). However, in our study, significant calcium transients and waves were distinctly correlated spatially and temporally with the application of ultrasound and only occurred in the presence of microbubbles (Optison). Furthermore, cell-to-cell contact is not necessary in all cases for calcium waves to occur (e.g., Sauer et al. 2000), such as in those cases with lower (e.g., <50%) cell confluency, paracrine factors in solution are involved in calcium waves.

All the cells were exposed to essentially the same ultrasound field, and yet significant response at the time of the ultrasound pulse was distinctly localized. The evidence was particularly striking when an intracellular calcium wave initiated from the side of the cell which was in the vicinity of a microbubble at the time of the ultrasound pulse (Figs. 3, 4). In other cells, the delayed initiation of $[Ca^{2+}]_i$ transients occurred as the result of a calcium wave long after the 0.2 s ultrasound pulse has passed, and was therefore not caused directly at the time of ultrasound application. Instead, the time scale (on the order of seconds) suggests that the cause is most likely the diffusion of a chemical agonist from the affected cells. The observed nonlinear, cell-to-cell movement of the wave in high confluency monolayers (e.g., Fig. 3) indicates the involvement of intracellular diffusion of a messenger through gap junctions in these cases. However, the significant damage to some cells will certainly release extracellular messengers like ATP to surrounding cells. In some cases, we have also observed slow propagation of the calcium wave without clear cell-to-cell contact, also suggesting an extracellular agent (Kumon et al., 2007a).

Considering the speed of the calcium wave (10–12 μm/s), the effects of the ultrasound induced bulk fluid movement (<2 μm/s) in our experiment on the diffusion of an extracellular factor, if it were released, is unlikely to be significant. However, whether ultrasound-induced higher local flow in the form of acoustic micro-streaming near cells or boundaries has significant effect on the direction of calcium wave propagation remained to be investigated.

The current study demonstrates that ultrasound can generate calcium transients and waves in the presence of microbubbles, but additional work is needed to understand the detailed mechanisms involved and possible biophysical and clinical consequences, an important task considering the wide spread use of ultrasound for imaging and interventional applications. For example, it has been suggested that extrasystoles during contrast-echocardiography may be triggered by Ca^{2+} influxes (Juffermans et al., 2006) and that prenatal exposure to ultrasound may have effects on neuronal migration in mice (Ang et al., 2006), although the exact mechanisms for these effects is not known.

CONCLUSION

Ratiometric fluorescence calcium imaging has revealed spatiotemporal calcium activities generated by ultrasound-mediated microbubble–cell interactions. In physiological $[Ca^{2+}]_o$, cells immediately affected by ultrasound application in the presence of microbubbles showed either (i) a rapid rise in $[Ca^{2+}]_i$ followed by a longer decay back to the original level or (ii) a failure to recover. Intracellular $[Ca^{2+}]$ oscillations and intercellular calcium waves were often observed in surrounding cells. In Ca^{2+}-free solution, cells that were affected by ultrasound did not recover to their initial $[Ca^{2+}]_i$. Focal, immediate effects due to ultrasound application were observed in some cells, while other cells in the vicinity experience delayed changes in $[Ca^{2+}]_i$ even after the end of ultrasound duration. The spatial extent of these delayed effects can be 100 μm or more from a single microbubble–cell interaction and over an even wider area when there are interactions with multiple cells. These delayed effects can also last for several minutes after the ultrasound is applied. Further studies are necessary to determine the detailed mechanisms involved and the significance of the demonstrated Ca^{2+} activities for biomedical ultrasound applications including ultrasound-mediated drug and gene delivery.

Acknowledgements

The authors would like to acknowledge Yun Zhou for technical assistance and Olivier Izad for cell culture. This work was supported in part by National Institutes of Health (R01CA116592 to C. X. Deng).

References

Ang ES Jr, Gluncic V, Duque A, Schafer ME, Rakic P. Prenatal exposure to ultrasound waves impacts neuronal migration in mice. Proc Natl Acad Sci USA 2006;103:12903–10. [PubMed: 16901978]

Bekeredjian R, Bohris C, Hansen A, Katus HA, Kuecherer HF, Hardt SE. Impact of microbubbles on shock wave-mediated DNA uptake in cells in vitro. Ultrasound Med Biol 2007;33:743–50. [PubMed: 17383800]

Berridge MJ, Bootman MD, Roderick HL. Calcium signalling: dynamics, homeostasis and remodelling. Nat Rev Mol Cell Biol 2003;4:517–29. [PubMed: 12838335]

Boitano S, Dirksen ER, Sanderson MJ. Intercellular propagation of calcium waves mediated by inositol trisphosphate. Science 1992;258:292–5. [PubMed: 1411526]

Campbell P, Prausnitz MR. Future directions for therapeutic ultrasound. Ultrasound Med Biol 2007;33:657. [PubMed: 17343978]

Davies PF. Flow-mediated endothelial mechanotransduction. Physiol Rev 1995;75:519–60. [PubMed: 7624393]

Deng CX, Sieling F, Pan H, Cui J. Ultrasound-induced cell membrane porosity. Ultrasound Med Biol 2004;30:519–26. [PubMed: 15121254]

Enomoto K, Furuya K, Yamagishi S, Maeno T. Mechanically induced electrical and intracellular calcium responses in normal and cancerous mammary cells. Cell Calcium 1992;13:501–11. [PubMed: 1423530]

Feril LB Jr, Ogawa R, Tachibana K, Kondo T. Optimized ultrasound-mediated gene transfection in cancer cells. Cancer Sci 2006;97:1111–4. [PubMed: 16925580]

Ferrara K, Pollard R, Borden M. Ultrasound microbubble contrast agents: fundamentals and application to gene and drug delivery. Annu Rev Biomed Eng 2007;9:415–47. [PubMed: 17651012]

Gamper N, Stockand JD, Shapiro MS. The use of Chinese hamster ovary (CHO) cells in the study of ion channels. J Pharmacol Toxicol Methods 2005;51:177–85. [PubMed: 15862463]

Geiger RV, Berk BC, Alexander RW, Nerem RM. Flow-induced calcium transients in single endothelial cells: spatial and temporal analysis. Am J Physiol 1992;262:C1411–7. [PubMed: 1616008]

Grynkiewicz G, Poenie M, Tsien RY. A new generation of Ca^{2+} indicators with greatly improved fluorescence properties. J Biol Chem 1985;260:3440–50. [PubMed: 3838314]

Hallow DM, Mahajan AD, Prausnitz MR. Ultrasonically targeted delivery into endothelial and smooth muscle cells in ex vivo arteries. J Control Release 2007;118:285–93. [PubMed: 17291619]

Honda H, Kondo T, Zhao QL, Feril LB Jr, Kitagawa H. Role of intracellular calcium ions and reactive oxygen species in apoptosis induced by ultrasound. Ultrasound Med Biol 2004;30:683–92. [PubMed: 15183235]

Huang JB, Kindzelskii AL, Clark AJ, Petty HR. Identification of channels promoting calcium spikes and waves in HT1080 tumor cells: their apparent roles in cell motility and invasion. Cancer Res 2004;64:2482–9. [PubMed: 15059902]

Juffermans LJ, Dijkmans PA, Musters RJ, Visser CA, Kamp O. Transient permeabilization of cell membranes by ultrasound-exposed microbubbles is related to formation of hydrogen peroxide. Am J Physiol Heart Circ Physiol 2006;291:H1595–601. [PubMed: 16632548]

Kono T, Nishikori T, Kataoka H, Uchio Y, Ochi M, Enomoto K. Spontaneous oscillation and mechanically induced calcium waves in chondrocytes. Cell Biochem Funct 2006;24:103–11. [PubMed: 16342135]

Kudo, N.; Miyaoka, T.; Okada, K.; Yamamoto, K.; Niwa, K. Study on mechanism of cell damage caused by microbubbles exposed to ultrasound. In: Yuhas, DE.; Schneider, SC., editors. IEEE Ultrasonics Symposium Proceedings. Vol. 2. Piscataway, NJ: IEEE; 2002. p. 1383-1386.

Kumon RE, Aehle M, Sabens D, Parikh P, Kourennyi D, Deng CX. Ultrasound-induced calcium oscillations and waves in Chinese hamster ovary cells in the presence of microbubbles. Biophys J 2007a;93:L29–31. [PubMed: 17631537]

Kumon, RE.; Parikh, P.; Sabens, D.; Aehle, M.; Kourennyi, D.; Deng, CX. Measuring and Modeling Sonoporation Dynamics in Mammalian Cells via Calcium Imaging. In: Coussios, C-C.; ter, Haar G., editors. Therapeutic Ultrasound: 6th International Symposium on Therapeutic Ultrasound. Vol. 911. New York: American Institute of Physics; 2007b. p. 484-491.

McNeil PL, Kirchhausen T. An emergency response team for membrane repair. Nat Rev Mol Cell Biol 2005;6:499–505. [PubMed: 15928713]

McNeil PL, Steinhardt RA. Loss, restoration, and maintenance of plasma membrane integrity. J Cell Biol 1997;137:1–4. [PubMed: 9105031]

McNeil PL, Steinhardt RA. Plasma membrane disruption: repair, prevention, adaptation. Annu Rev Cell Dev Biol 2003;19:697–731. [PubMed: 14570587]

Mehier-Humbert S, Yan F, Frinking P, Schneider M, Guy RH, Bettinger T. Ultrasound-mediated gene delivery: influence of contrast agent on transfection. Bioconjug Chem 2007;18:652–62. [PubMed: 17419583]

Miller DL, Pislaru SV, Greenleaf JE. Sonoporation: mechanical DNA delivery by ultrasonic cavitation. Somat Cell Mol Genet 2002;27:115–34. [PubMed: 12774945]

Mortimer AJ, Dyson M. The effect of therapeutic ultrasound on calcium uptake in fibroblasts. Ultrasound Med Biol 1988;14:499–506. [PubMed: 3227573]

Newman CM, Bettinger T. Gene therapy progress and prospects: Ultrasound for gene transfer. Gene Ther 2007;14:465–475. [PubMed: 17339881]

Ohl CD, Arora M, Ikink R, de Jong N, Versluis M, Delius M, et al. Sonoporation from jetting cavitation bubbles. Biophys J 2006;91:4285–95. [PubMed: 16950843]

Paliwal S, Mitragotri S. Ultrasound-induced cavitation: applications in drug and gene delivery. Expert Opin Drug Deliv 2006;3:713–26. [PubMed: 17076594]

Parvizi J, Parpura V, Greenleaf JF, Bolander ME. Calcium signaling is required for ultrasound-stimulated aggrecan synthesis by rat chondrocytes. J Orthop Res 2002;20:51–7. [PubMed: 11853090]

Petty HR. Spatiotemporal chemical dynamics in living cells: from information trafficking to cell physiology. Biosystems 2006;83:217–24. [PubMed: 16236427]

Postema M, Bouakaz A, Versluis M, de Jong N. Ultrasound-induced gas release from contrast agent microbubbles. IEEE Trans Ultrason Ferroelectr Freq Control 2005;52:1035–41. [PubMed: 16118985]

Postema M, van Wamel A, Lancee CT, de Jong N. Ultrasound-induced encapsulated microbubble phenomena. Ultrasound Med Biol 2004;30:827–40. [PubMed: 15219962]

Prentice P, Cuschieri A, Dholakia K, Prausnitz M, Campbell P. Membrane disruption by optically controlled microbubble cavitation. Nature Physics 2005;1:107–110.

Sabens, D.; Aehle, M.; Steyer, G.; Kourennyi, D.; Deng, CX. Calcium Imaging of Sonoporation of Mammalian Cells. In: Clement, GT.; McDannold, NJ.; Hynynen, K., editors. Therapeutic Ultrasound: 5th International Symposium on Therapeutic Ultrasound. Vol. 829. Boston, MA: American Institute of Physics; 2006. p. 533-537.

Sanderson MJ, Charles AC, Boitano S, Dirksen ER. Mechanisms and function of intercellular calcium signaling. Mol Cell Endocrinol 1994;98:173–87. [PubMed: 8143927]

Sanderson MJ, Charles AC, Dirksen ER. Mechanical stimulation and intercellular communication increases intracellular Ca^{2+} in epithelial cells. Cell Regul 1990;1:585–96. [PubMed: 2078569]

Sauer H, Hescheler J, Wartenberg M. Mechanical strain-induced Ca^{2+} waves are propagated via ATP release and purinergic receptor activation. Am J Physiol Cell Physiol 2000;279:C295–307. [PubMed: 10912995]

Schlicher RK, Radhakrishna H, Tolentino TP, Apkarian RP, Zarnitsyn V, Prausnitz MR. Mechanism of intracellular delivery by acoustic cavitation. Ultrasound Med Biol 2006;32:915–24. [PubMed: 16785013]

Steinhardt RA. The mechanisms of cell membrane repair: A tutorial guide to key experiments. Ann N Y Acad Sci 2005;1066:152–65. [PubMed: 16533925]

Sundaram J, Mellein BR, Mitragotri S. An experimental and theoretical analysis of ultrasound-induced permeabilization of cell membranes. Biophys J 2003;84:3087–101. [PubMed: 12719239]

Taylor SL, Rahim AA, Bush NL, Bamber JC, Porter CD. Targeted retroviral gene delivery using ultrasound. J Gene Med 2007;9:77–87. [PubMed: 17310476]

Togo T, Alderton JM, Bi GQ, Steinhardt RA. The mechanism of facilitated cell membrane resealing. J Cell Sci 1999;112 (Pt 5):719–31. [PubMed: 9973606]

Togo T, Krasieva TB, Steinhardt RA. A decrease in membrane tension precedes successful cell-membrane repair. Mol Biol Cell 2000;11:4339–46. [PubMed: 11102527]

Tran TA, Roger S, Le Guennec JY, Tranquart F, Bouakaz A. Effect of ultrasound-activated microbubbles on the cell electrophysiological properties. Ultrasound Med Biol 2007;33:158–63. [PubMed: 17189059]

Tsukamoto, A.; Ushida, T.; Yasui, N.; Watanabe, Y.; Furukawa, K.; Tateishi, T. Traveling wave sonication evokes intracellular [Ca^{2+}] transients in muine fibroblasts. In: ter Haar, GR.; Rivens, I., editors. Therapeutic Ultrasound: 4th International Symposium on Therapeutic Ultrasound. Vol. 754. New York: American Institute of Physics; 2005. p. 269-271.

van Wamel A, Kooiman K, Emmer M, ten Cate FJ, Versluis M, de Jong N. Ultrasound microbubble induced endothelial cell permeability. J Control Release 2006a;116:e100–2. [PubMed: 17718938]

van Wamel A, Kooiman K, Harteveld M, Emmer M, ten Cate FJ, Versluis M, et al. Vibrating microbubbles poking individual cells: drug transfer into cells via sonoporation. J Control Release 2006b;112:149–55. [PubMed: 16556469]

Wu, J.; Nyborg, WL., editors. Emerging therapeutic ultrasound. Hackensack, NJ, USA: World Scientific; 2007.

Yellowley CE, Jacobs CR, Li Z, Zhou Z, Donahue HJ. Effects of fluid flow on intracellular calcium in bovine articular chondrocytes. Am J Physiol 1997;273:C30–6. [PubMed: 9252439]

Zhou Y, Cui J, Deng CX. Dynamics of sonoporation correlated with acoustic cavitation activities. Biophys J 2008a;94:L51–3. [PubMed: 18212008]

Zhou Y, Shi J, Cui J, Deng CX. Effects of extracellular calcium on cell membrane resealing in sonoporation. J Control Release 2008b;126:34–43. [PubMed: 18158198]

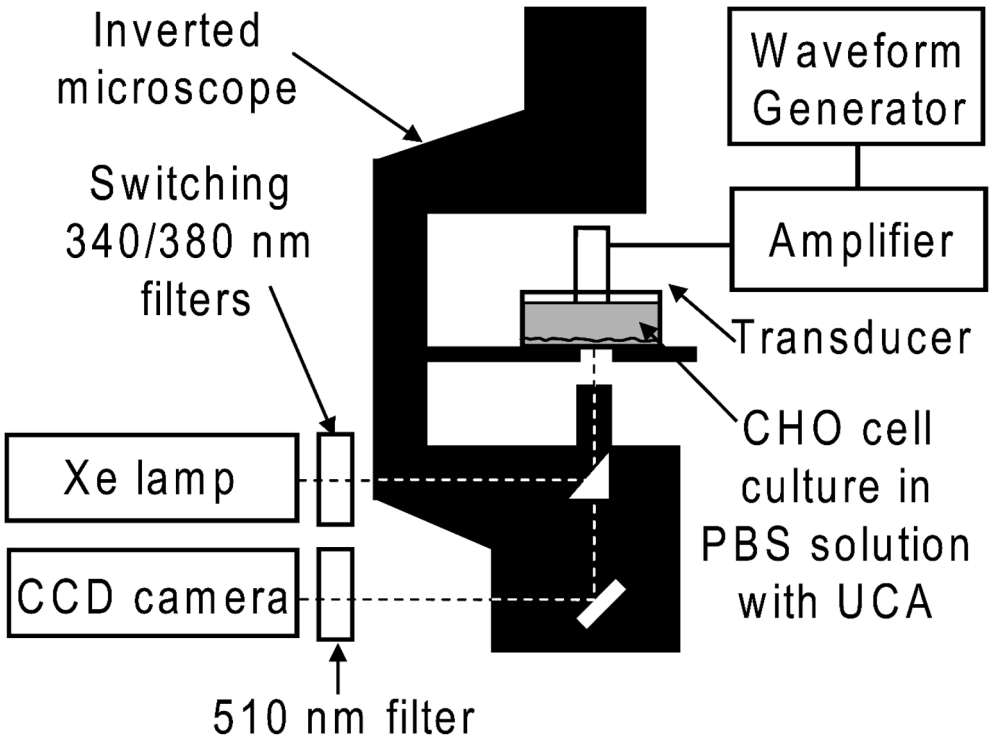

Figure 1.
Schematic diagram of experimental setup for ratiometric calcium imaging of sonoporation. The setup includes an inverted microscope and a Lamda DG-4 system for dual-wavelength exicitation. (CCD: charge-coupled device, CHO: Chinese hamster ovary, PBS: phosphate-buffered saline, UCA: ultrasound contrast agent).

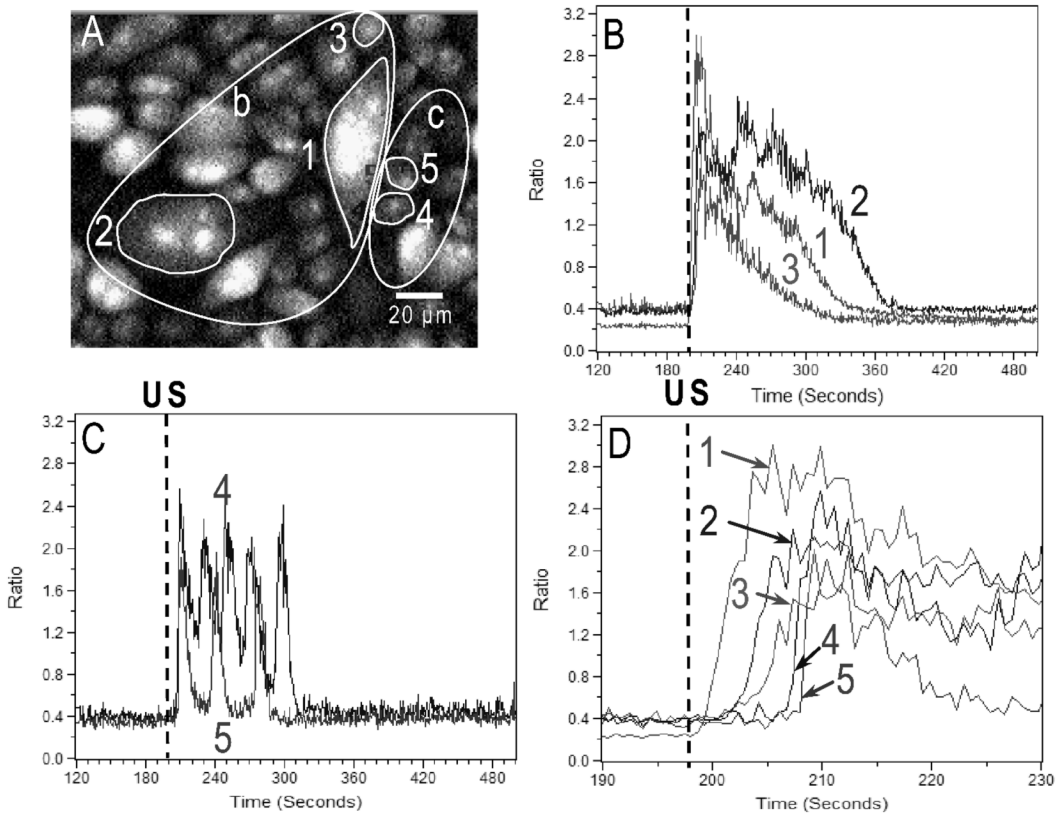

Figure 2.

Intracellular calcium ion transients in selected cells induced by an ultrasound pulse in solution with $[Ca^{2+}]_o$ = 0.9 mM. The transients are plotted in terms of the fura-2 fluorescence intensity ratio $R = F_{340}/F_{380}$. An ultrasound (US) pulse was applied at 199 s. (A) Background-corrected fluorescence image from 380 nm excitation with manually-segmented cell regions shown in B and C. (B) Transients of cells with various recovery durations. (C) Other cells (e.g. Cells 4 and 5) adjacent to Cell 1 exhibit large amplitude oscillations with differing periods and numbers of oscillation cycles. The responses are delayed compared to those cells in B. (D) Transients of all selected cells over smaller time range, showing that Cell 1 responds immediately after the ultrasound application, while the response of the other cells is delayed.

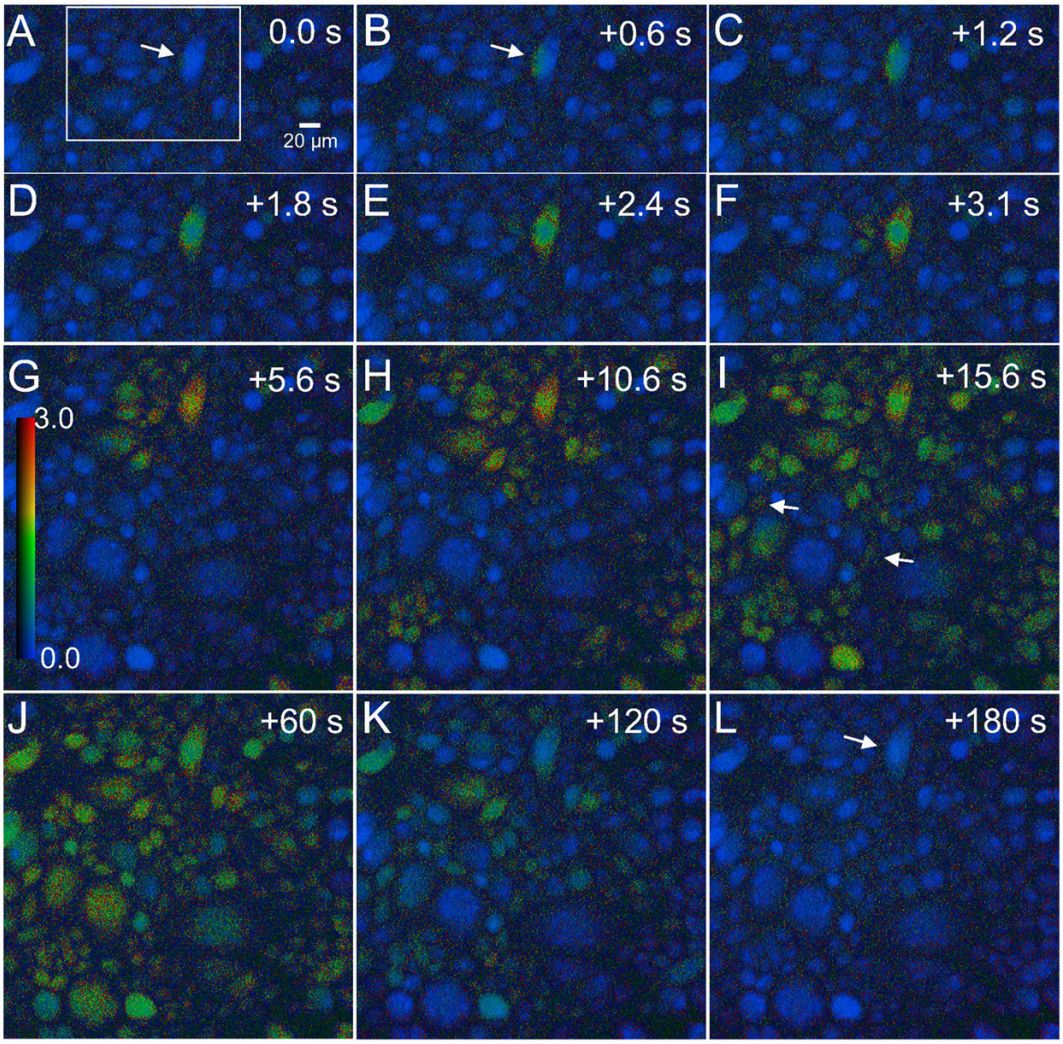

Figure 3.

Time-lapse ratio images showing calcium waves induced by ultrasound pulse for cells in solution with $[Ca]_o$ = 0.9 mM including the cells in Fig. 2. The color bar indicates the local fura-2 fluorescence ratio $R = F_{340}/F_{380}$. The labels in the upper right corner of each image list the time since the first image. The images before ultrasound application show variation in baseline fluorescence intensity within different cells. (A) Ratio image before ultrasound pulse. The white rectangle shows the cells in Fig. 2, while the arrow points to the cell that will be immediately affected by the ultrasound pulse (Cell 1 in Fig. 2). (B) Ratio image at first frame after ultrasound pulse (duration 0.2 s). The first significant change is seen in only one cell (arrow). Subsequent ratio images show (C–E) propagation of an intracellular wave, (F–J) propagation of intercellular calcium waves originating from this immediately-affected cell and locations likely from outside the field of view. Arrows in (I) indicate examples of locations showing cell-to-cell propagation of the calcium wave, connecting the two calcium transient regions in the image, (K) dissipation of the calcium waves, and (L) full recovery of all the cells in the field of view. Note that the immediately-affected cell also recovers (arrow).

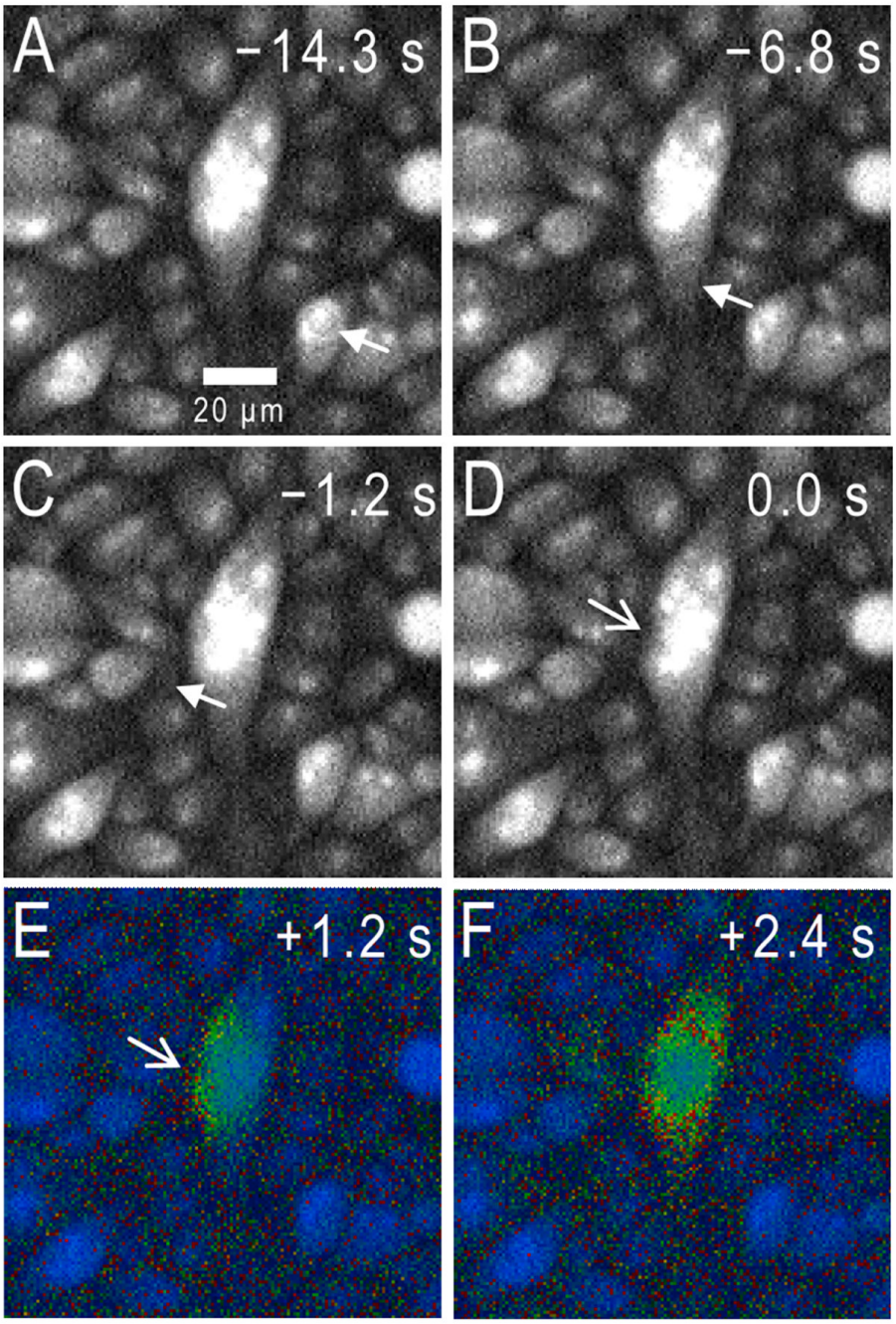

Figure 4.

Examples of microbubble in the vicinity of the cells that first exhibit Ca^{2+} changes in Figure 3, as shown by background-corrected fluorescence images from 380 nm excitation. (A–C) Prior to ultrasound exposure, the spherical microbubble (closed arrows) scatters light as it moves through the solution above the cells. (D) Immediately after ultrasound exposure the microbubble has disappeared and a calcium wave is initiated in an adjacent cell (open arrow; compare with Fig. 3A). (E–F) Ratiometric images after ultrasound was applied showing the change in calcium (enlarged sub-images of Fig. 3C, E using the same color scale).

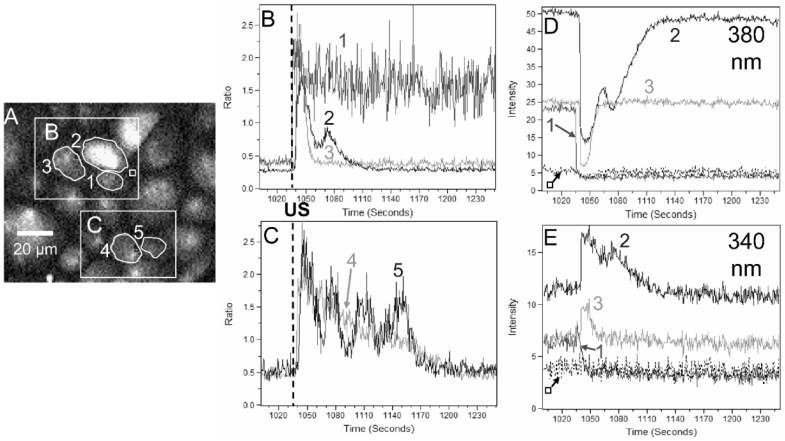

Figure 5.

Intracellular calcium ion transients induced by an ultrasound pulse for selected cells in solution with $[Ca^{2+}]_o$ = 0.9 mM from a different culture, showing a non-recovering cell. The transients are plotted in terms of the fura-2 fluorescence intensity ratio $R = F_{340}/F_{380}$. An ultrasound (US) pulse was applied at 1035 s. (A) Background-corrected fluorescence image from 380 nm excitation with manually-segmented cell regions shown in B–D. (B) Transients of cells that do not recover (Cell 1), recover with a superimposed oscillation (Cell 2), and recover monotonically (Cell 3). Only Cell 1 responds immediately at the time of ultrasound application, while the response of the other cells is delayed. (C) More distant cells with slow transient decay without (Cell 4) and with (Cell 5) oscillations. These cells respond later than those in B. (D–E) Fluorescence intensities at 510 nm due to excitations at 380 nm or 340 nm (solid) and adjacent cell-free region (dashed) for the cells in graph B.

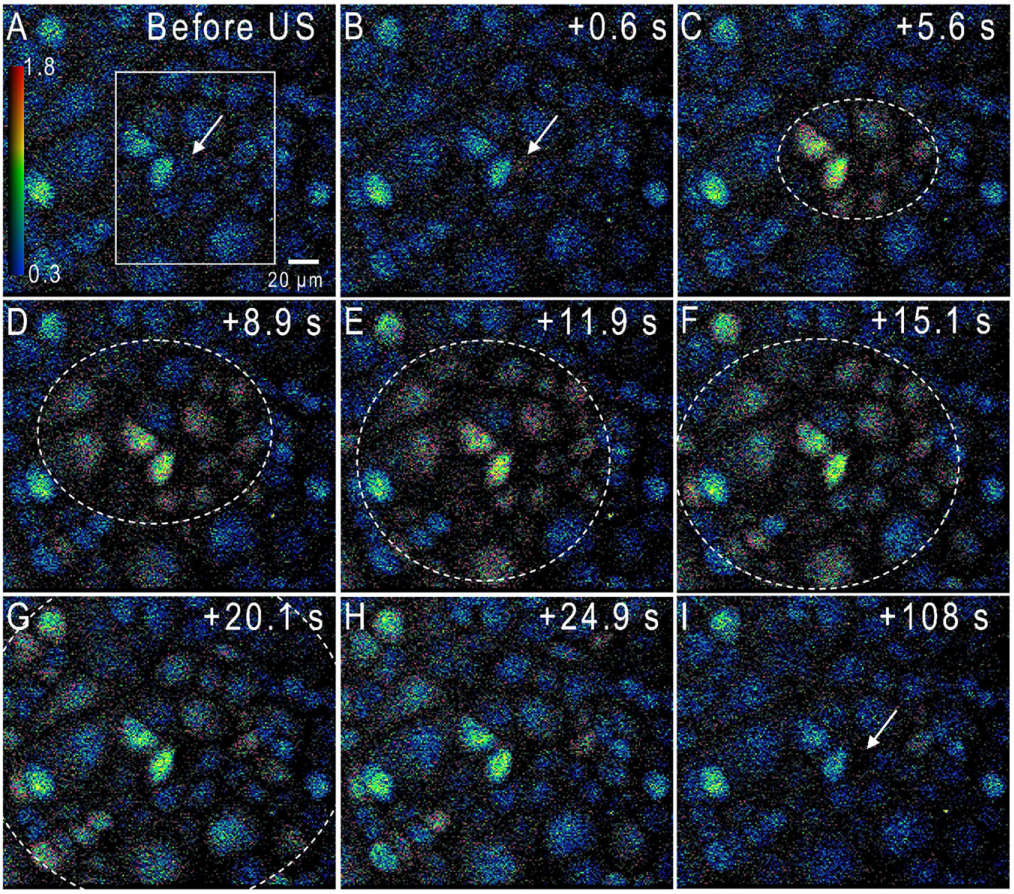

Figure 6.

Time-lapse ratio images of calcium wave induced by ultrasound pulse for cells in extracellular $[Ca]_o$ = 0.9 mM, including the cells in Fig. 5. The color bar indicates the local fura-2 fluorescence ratio $R = F_{340}/F_{380}$. The labels in the upper right corner of each image list the time since the initial image. (A) Ratio image before ultrasound pulse (duration 0.2 s). The white rectangle shows the cells in Fig. 4, while the arrow points to the only cell (Cell 1 in Fig. 5) that is immediately affected by the ultrasound pulse in the next frame. (B) Ratio image at first frame after ultrasound pulse. The first significant change is seen in only one cell (arrow). (C–H) Ratio images at subsequent times show approximately elliptical calcium wave expanding out from the first cell immediately affected in B. (I) Ratio image after full recovery of all the cells in the field of view. The immediately-affected cell does not recover (arrow pointing to a dark region without fluorescence signals).

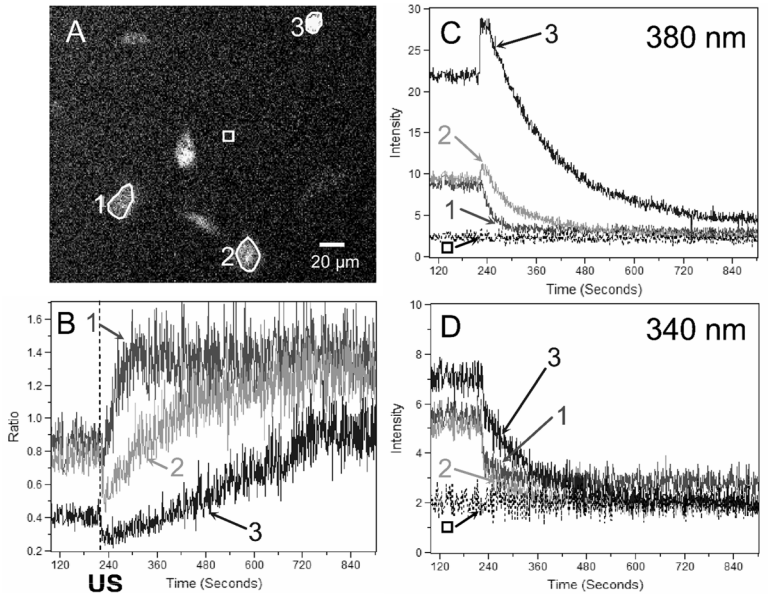

Figure 7.

Intracellular calcium ion transients for cells in extracellular $[Ca^{2+}]_o$ = 0 mM. The transients are plotted in terms of the fura-2 fluorescence intensity ratio $R = F_{340}/F_{380}$. An ultrasound (US) pulse was applied at 222 s. (A) Background-corrected fluorescence image from 380 nm excitation with manually-segmented cell regions shown in B and C. (B) Transients of cells with various recovery durations. (C–D) Fluorescence intensities at 510 nm due to excitations at 380 nm or 340 nm (solid) and adjacent cell-free region (dashed) for the cells in graph B.